METEOROLOGICAL APPLICATIONS
Meteorol. Appl. **23**: 101–114 (2016)
Published online 25 November 2015 in Wiley Online Library
(wileyonlinelibrary.com) DOI: 10.1002/met.1534

RMetS
Royal Meteorological Society

Performance of super high resolution numerical weather prediction model in forecasting terrain-disrupted airflow at the Hong Kong International Airport: case studies

P. W. Chan* and K. K. Hon
Hong Kong Observatory, China

ABSTRACT: Hong Kong International Airport (HKIA) is situated in an area of complex terrain. Mountains near the airport can lead to terrain-disrupted airflow disturbances, which may bring about hazardous weather phenomena for aviation, such as low-level windshear and turbulence. Timely forecasting of such airflow disturbances would be useful in providing early warnings to the pilots. The Hong Kong Observatory has been running a super high resolution numerical weather prediction model suite, the aviation model (AVM), since late 2013, with spatial resolution up to 200 m immediately around HKIA. After testing and tuning over the past year, the performance of the AVM in forecasting terrain-disrupted airflow at the airport area is investigated in this study. Two typical cases of such complex airflow are considered, Foehn wind and mountain wave. The AVM is found to capture successfully some salient features of the airflow as observed around HKIA through comparison with light detection and ranging (LIDAR) and weather buoy observations. The model also helps in shedding new light on the airflow from the vertical cross sections of the winds across the mountains. Limitations of the AVM are also discussed.

KEY WORDS forecasting; modelling; hazards; remote sensing

Received 12 March 2015; Revised 12 June 2015; Accepted 23 June 2015

1. Introduction

Hong Kong International Airport (HKIA) is situated in an area of complex terrain. It is built on a reclaimed island to the north of Lantau Island (Figure 1), which has peaks as high as 1000 m above mean sea level (amsl) and valleys as low as 400 m amsl in between. Winds blowing over the complex terrain of Lantau Island may lead to airflow disturbances over HKIA. Such terrain-disrupted airflow could be hazardous to the aircraft landing at or departing from the airport. It may bring about low-level windshear and turbulence to be encountered by the aircraft. There is a number of recent papers on the observation and modelling of terrain-disrupted airflow, especially in relation to the occurrence of low-level windshear and turbulence encountered by the aircraft. For instance, Carruthers *et al.* (2014) consider the use of a numerical model to predict downslope flow. Chan (2014b) and Hon and Chan (2014) discuss the observation of windshear and turbulence using Doppler light detection and ranging (LIDAR) systems. Lee and Chan (2014) also discuss the application of LIDAR for windshear detection using the so-called *F*-factor based on the LIDAR system's headwind profiles.

In order to monitor the terrain-disrupted airflow over the airport, the Hong Kong Observatory (HKO) operates a suite of meteorological instruments inside and around HKIA. They consist of both *in situ* and ground-based remote sensing equipment. Their locations are indicated in Figure 1. In particular, the ground-based anemometers and weather buoys over the waters around the airport help visualize the wind pattern in the airport area and the airflow near the surface. The airflow at higher elevations within the boundary layer of the troposphere can be monitored using the Doppler LIDAR systems. There are two LIDAR systems operating at HKIA, each located near either of the two runways of the airport. They perform plan position indicator (PPI) scans at elevation angles of 3° and 6° above the horizon, providing information about the distribution of the radial wind velocity in the airport area (up to 10 km away from the LIDAR system). The two elevation angles are chosen so that the scanning areas are close to the flight paths of the landing and the departing aircraft. Many phenomena of terrain-disrupted airflow have been captured by this equipment, including Foehn wind (Chan, 2014a) and mountain wave (Shun *et al.*, 2004).

Apart from real-time monitoring, the HKO also attempts to forecast the occurrence of terrain-induced airflow disturbances and thus the possibility of low-level windshear and turbulence, in order to provide early alerts to pilots about any disrupted airflow. An aviation model (AVM) has been set up to run in real time since late 2013. It is based on the weather research and forecasting (WRF) model, running at a resolution of 600 m over the Pearl River Delta (PRD) area and at a resolution of 200 m near the airport. The model has been fine-tuned around 2014 and has become more stable since early 2015.

This study discusses the performance of the AVM in forecasting typical cases of terrain-disrupted airflow disturbances at HKIA as observed by the LIDAR systems and anemometers/weather buoys, namely Foehn wind and mountain wave. The typical features of the airflow disturbances are examined (using more recent cases in 2015) and the forecasting capabilities of the AVM are described. When low-level windshear is expected for such an airflow pattern from, say, a glide-path scan windshear detection algorithm (GLYGA, with details from Shun and Chan, 2008), it would be compared with similar windshear forecasts

* Correspondence: P. W. Chan, Hong Kong Observatory, 134A Nathan Road, Kowloon, Hong Kong, China. E-mail: pwchan@hko.gov.hk

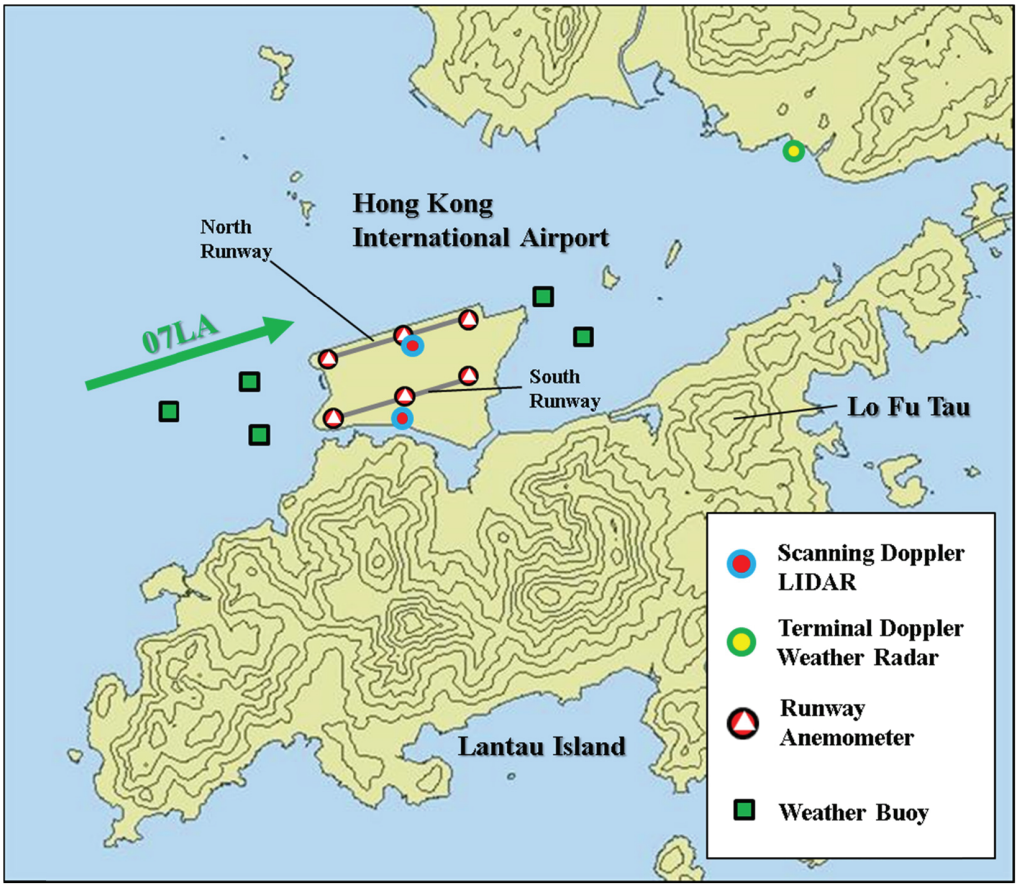

Figure 1. Selected meteorological instruments inside and around the Hong Kong International Airport (HKIA). The height contours are in 100 m. The length of each runway is about 3800 m, which can be used as a scale in this figure. Direction of arrival corridor 07LA is included for reference.

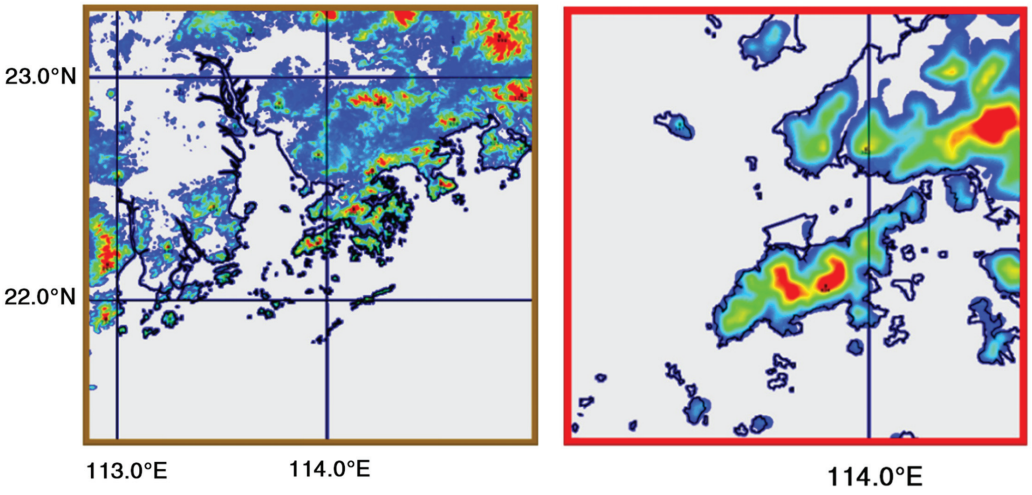

Figure 2. Schematic diagram of the two domains of the aviation model (AVM), AVM-PRD (left, horizontal resolution of 600 m) and AVM-HKA (right, horizontal resolution of 200 m). Terrain elevation indicated in colours (red corresponding to about 1000 m amsl).

based on the AVM (GLYGA-AVM). Through case studies, this research aims at summarizing the features that can be well captured by the super high spatial resolution of the numerical weather prediction (NWP) model and the limitations of the model forecasts. The results from the study are expected to be a useful reference for similar implementations of high-resolution NWP models at other airports situated in areas of complex terrain.

2. The aviation model

To support short-term, fine-scale weather forecasts for HKIA and its vicinity, the HKO began operating in real time a sub-kilometre resolution NWP model suite, the AVM, since late 2013. The AVM is based on version 3.4.1 of the WRF-ARW model (Skamarock and Klemp, 2007) and comprises two single-nested domains (Figure 2) – the AVM-PRD at 600 m resolution

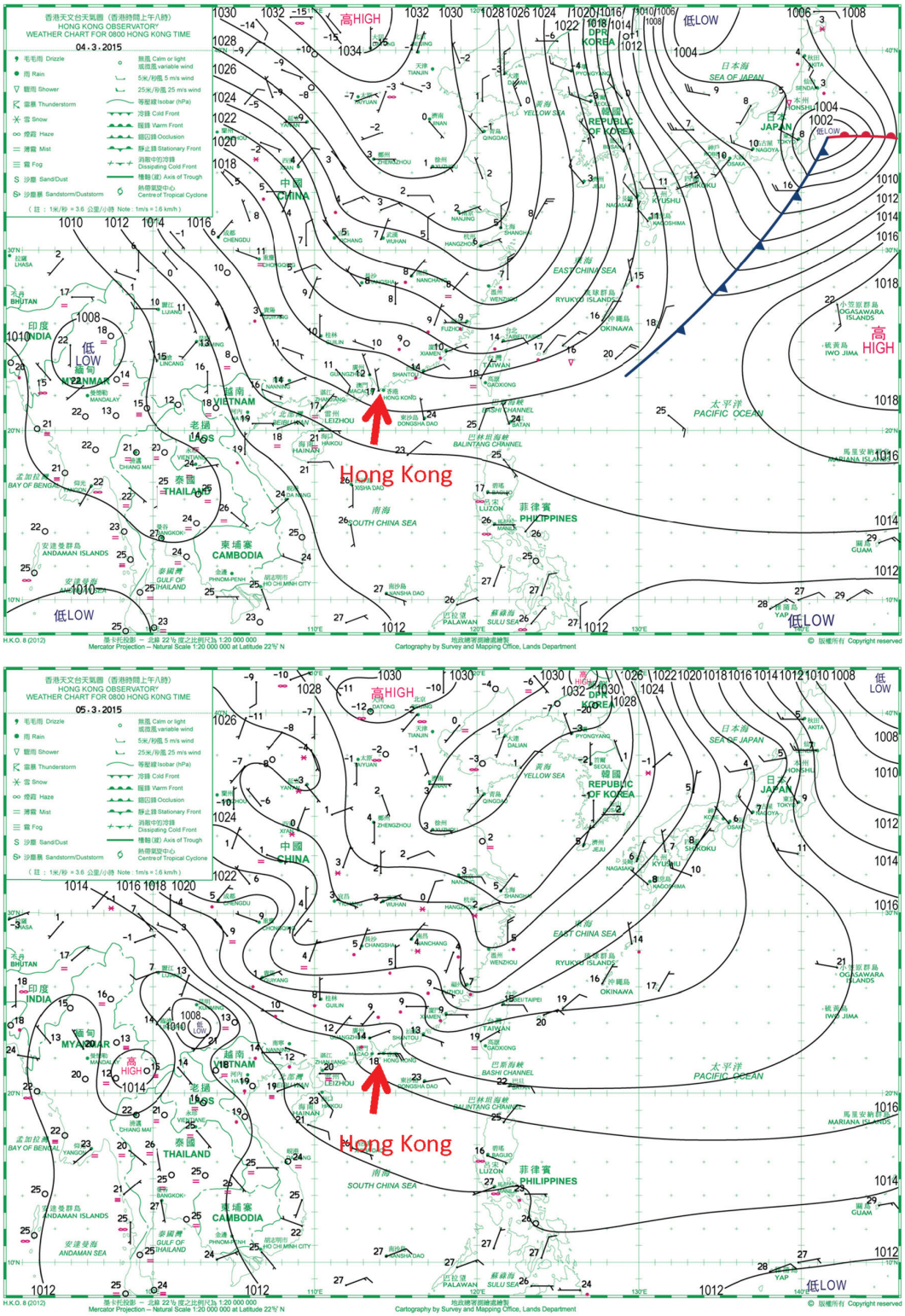

Figure 3. Surface isobaric charts at 0800 HKT on 4 March (a) and 5 March (b) 2015.

covering the Greater PRD region and the AVM-HKA at 200 m resolution covering HKIA and the western part of Hong Kong. A preliminary version of the AVM has been reported by Wong *et al.* (2013). Both domains are updated hourly and provide forecasts up to T + 7 regularly, where T indicates the analysis time.

The outer AVM-PRD domain has a size of about 350 km × 350 km (581 × 581 grid points), while the inner AVM-HKA domain covers about 50 km × 50 km (253 × 253 grid points). To strike a balance between computational time, vertical resolution and numerical stability, 42 vertical (eta) levels are used, with ∼10 layers in the lowest 1500 m of the model domain. The outer and inner domains are integrated at time steps of ∼12 and 3 s, respectively. Key model physics options include the rapid radiative transfer model for long wave and short wave

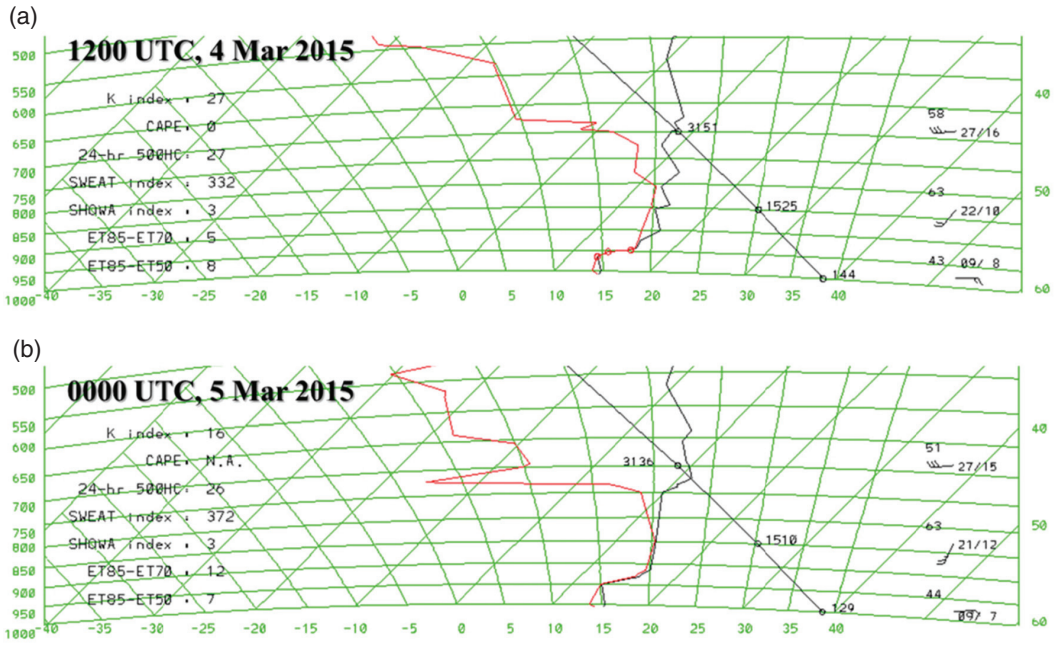

Figure 4. Radiosonde ascent at (a) 2000 HKT on 4 March 2015, and (b) 0800 HKT on 5 March 2015.

radiation, explicit cumulus convection and the NOAH land surface model. In particular, the large-eddy simulation (LES) mode of the WRF model is used in place of planetary boundary layer parameterization in the inner domain.

Boundary conditions to the AVM-PRD are provided by RAPIDS-NHM, the 2 km mesoscale NWP model in operation at the HKO. Technical details of RAPIDS-NHM can be found in Wong (2010). The initial conditions are generated using 3D-VAR analysis based on first guess (i.e. initial fields) provided by the mother models RAPIDS-NHM (for AVM-PRD) and AVM-PRD (for AVM-HKA). Data ingested include conventional surface and upper air observations, as well as a dense network of surface automatic weather stations over the inland Guangdong area.

In addition to conventional surface and upper air prognostic charts, specialized products have been developed using the high-resolution AVM-HKA output to assess the chance of significant windshear over HKIA runways. The GLYGA-AVM is essentially a LIDAR emulator and provides forecasted headwind profiles along the arrival and departure aircraft glide-paths as would be measured by the LIDAR scans. These forecasted headwind profiles are then processed using the same ramp detection algorithm as for LIDAR data to identify regions of sharp headwind changes. Such areas with the potential for significant windshear are then automatically highlighted for aviation forecasters' reference.

3. Foehn wind case, and the occurrence of low-level windshear and turbulence

Foehn wind occurs when there are east to southeasterly winds over the lower part of the boundary layer of the atmosphere with the presence of a temperature inversion near the top of the mountains of Lantau Island. A typical case occurred at HKIA during 4–5 March 2015. The surface isobaric charts at 0000 UTC (i.e. 0800 Hong Kong time, with HKT = UTC + 8 h) for these 2 days are given in Figure 3. On 4 March, southern China was under the influence of the northeast monsoon. A high pressure area on the surface gradually migrated to the east, so that a ridge of high pressure established itself over the southeastern coast of China on 5 March. This ridge brought about east to southeasterly winds of strong to gale force in the airport area.

The background atmosphere may be represented by the radiosonde measurements launched at King's Park, Hong Kong, which is located at about 20 km upstream of the HKIA in surface-based easterly flow. Figure 4 shows the wind direction, wind speed, temperature and dew point measurements from the radiosonde at 2000 HKT on 4 March and 0800 HKT on 5 March 2015. It could be seen that the surface winds were basically easterly, with the winds veering gradually with height. There is a low-level jet with wind speeds reaching $\sim$15 m s^{-1} at $\sim$500–700 m amsl, which is also about the height of the temperature inversion. The stable boundary layer together with the low-level jet would be favourable for the occurrence of Foehn wind at the airport area. It was raining at the radiosonde station on these 2 days, with hourly rainfall <1 mm.

Figure 5 shows the surface observations at the times when low-level windshear reports were received from the pilots. Between 0900 and 1000 HKT on 5 March 2015, there were six pilot reports over the runway corridor 07LA (approach to the north runway from the west) reporting windshear of headwind gain up to 13 m s^{-1} (25 kn) and headwind loss up to -10 m s^{-1} (-20 kn) as well as moderate turbulence between 1 and 4.6 km (2.5 nautical miles) from the runway threshold. Fresh to strong (Beaufort scale Force 5 and Force 6 to 7, respectively, namely, between 8.7 and 10.8 m s^{-1} (17 and 21 kn) and between 11.3 and 17 m s^{-1} (22 and 33 kn), respectively), east to southeasterly winds prevailed over the airport area. There is convergence between east-northeasterly winds and east-southeasterly winds (as indicated by weather buoys 1 and 2, WB1 and WB2) over the seas to the west of HKIA. Gale force winds (between 17.5 and 24.7 m s^{-1}, i.e. between 34 and 48 kn) were reported over the mountaintops and valleys in the western part of Lantau Island.

Figure 6 gives the time series of temperature, dew point, wind direction and wind speed of weather buoys WB1 and WB2 in the 2 day period (Hong Kong time). Both the buoys capture

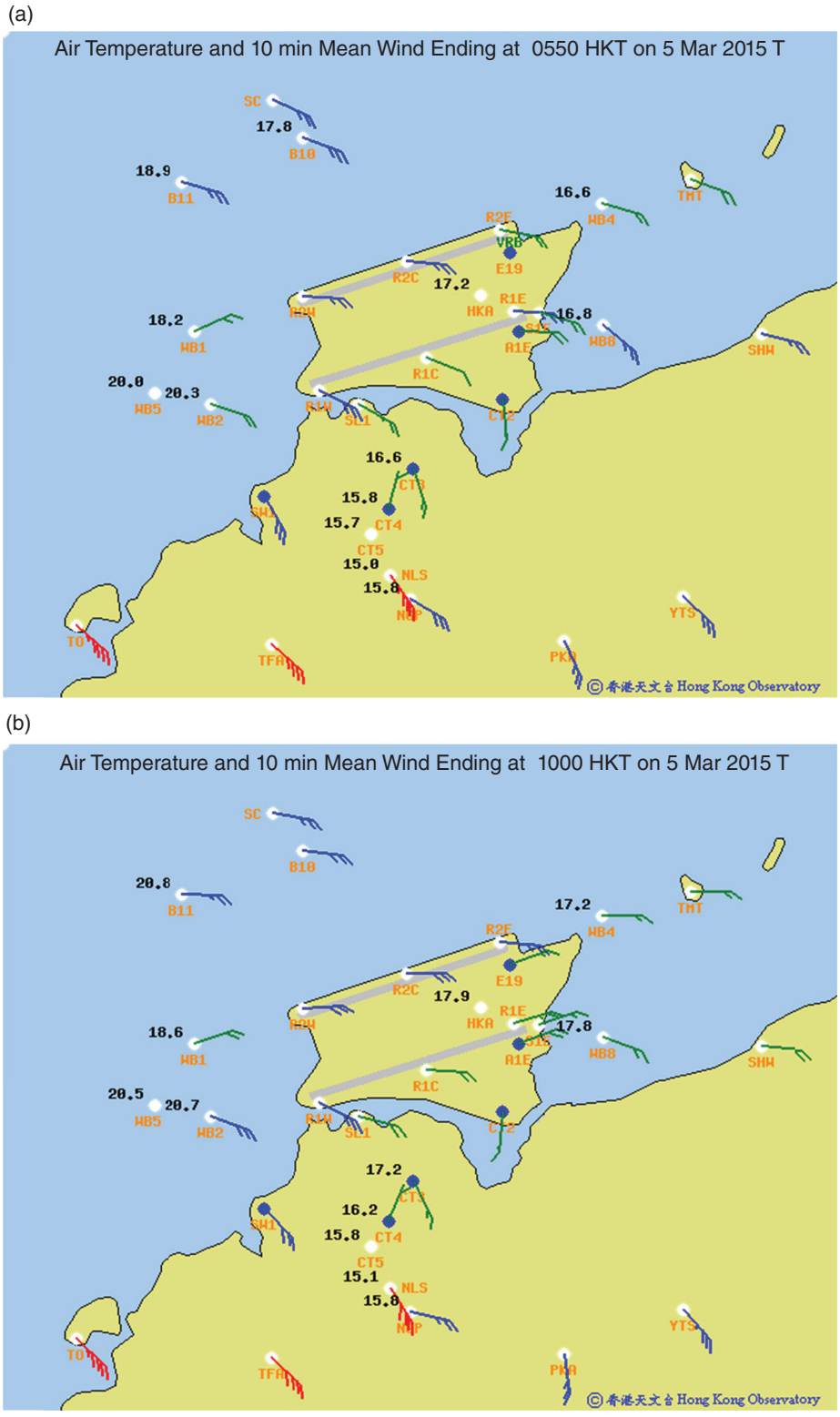

Figure 5. Surface wind measurements inside and around the Hong Kong International Airport (HKIA) at (a) 0550 HKT, 5 March 2015 and (b) 1000 HKT, 5 March 2015. Wind barbs are coloured according to wind strength (green for below 11.5 m s^{-1}, blue for 11.5–17.0 m s^{-1}, red for 17.5–24.0 m s^{-1}). The anemometer readings are 10 min mean winds. The temperature of buoy B11 is suspicious and could be wrong.

the establishment of Foehn wind, generally with 'pulsations' of temperature and dew point. They rise and fall up to 6 °C. There are corresponding changes in the wind direction, which is more apparent in WB2. The winds turn from the background east-northeasterly to northeasterly winds to become southeasterly, even to northerly. The occurrence of Foehn wind may match with the encountering of low-level windshear and turbulence by the aircrafts landing at the HKIA from the west.

In the present case, the dew point as registered by the weather buoys also increases during the Foehn event. A similar

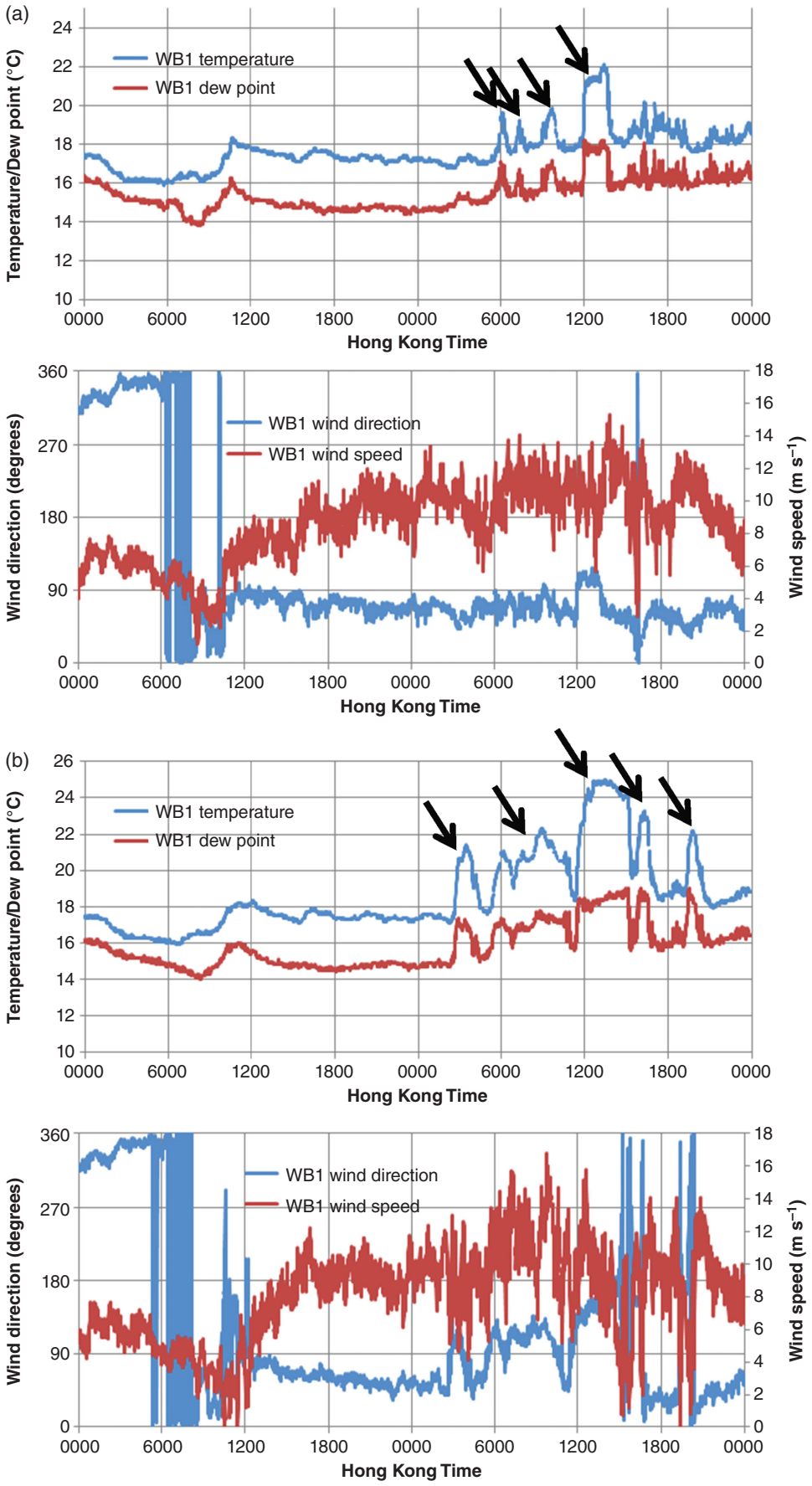

Figure 6. Time series of temperature, dew point, wind speed and wind direction of (a) WB1 and (b) WB2 in the period 4–5 March 2015. The values are 1 min averages. The Foehn wind periods are indicated by arrows.

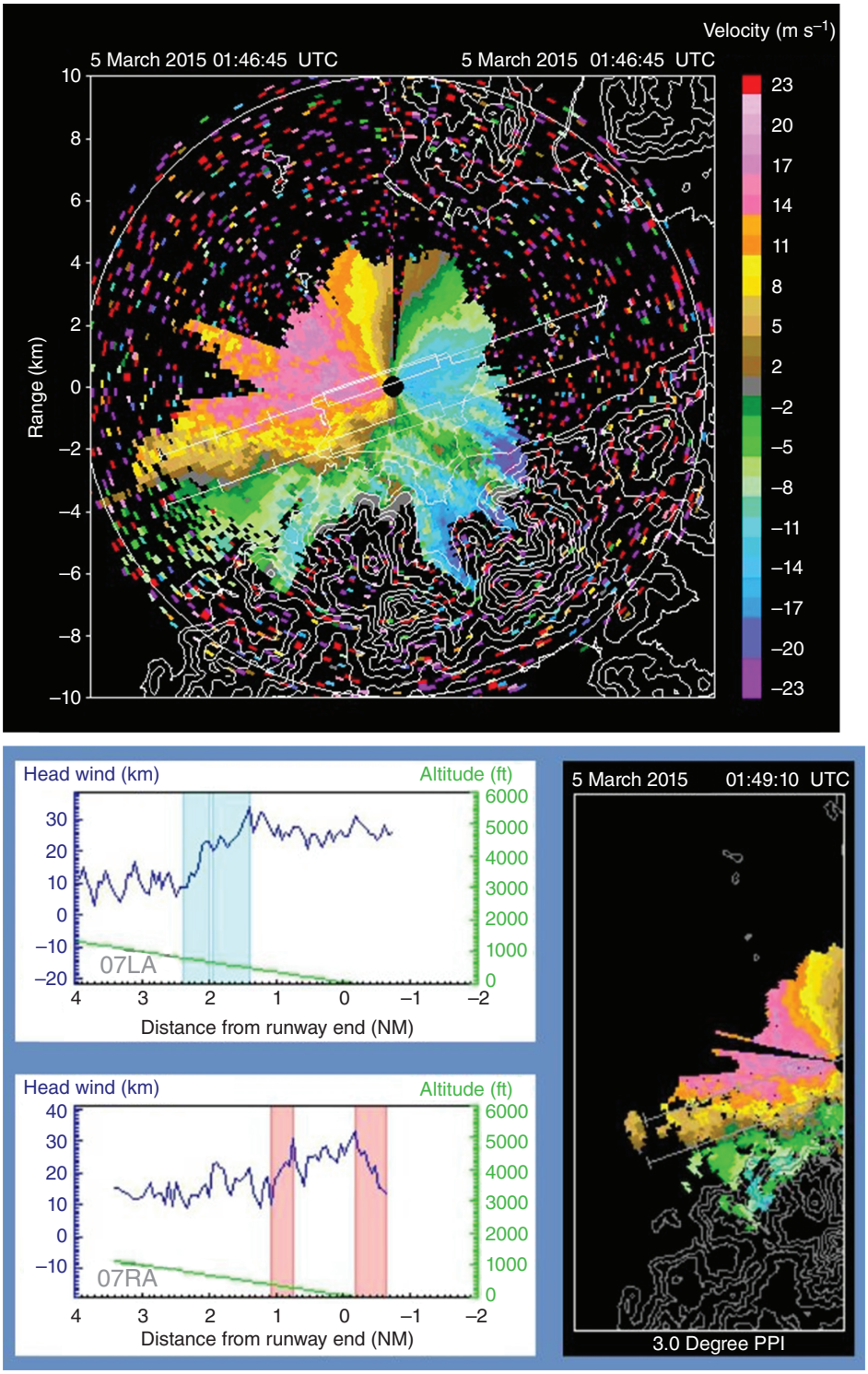

Figure 7. The 3° light detection and ranging (LIDAR) plan position indicator (PPI) scan of radial velocity (upper and lower right) and the headwind profiles as well as the windshear ramps (highlighted in red) at 07LA and 07RA runway corridors (lower left) at 0946 HKT, 5 March 2015.

observation has been documented in the literature, for example in Gaffin (2007). Whether this is a general phenomenon of the Foehn event in Hong Kong, has to be studied further by accumulating more observations of Foehn wind cases at HKIA. The dew point rise in the present case is ∼2 °C for mountains with heights of ∼1000 m on Lautau Island. This is consistent with the 2 °C threshold as adopted in Gaffin (2007), which states that 'the threshold of 2 °C was chosen because the surface dewpoint should theoretically rise (with the mixing ratio of the 850-hPa air mass conserved in an adiabatic descent) approximately 2 °C during a 1000-m descent'.

In the period from 0000 HKT, 4 March 2015, to 0000 HKT, 5 March 2015, there were >60 reports of low-level windshear by the pilots. The LIDAR observations at these time points of windshear/turbulence encounters can be seen in Figure 7. From the PPI scans of the north runway LIDAR system, it could be

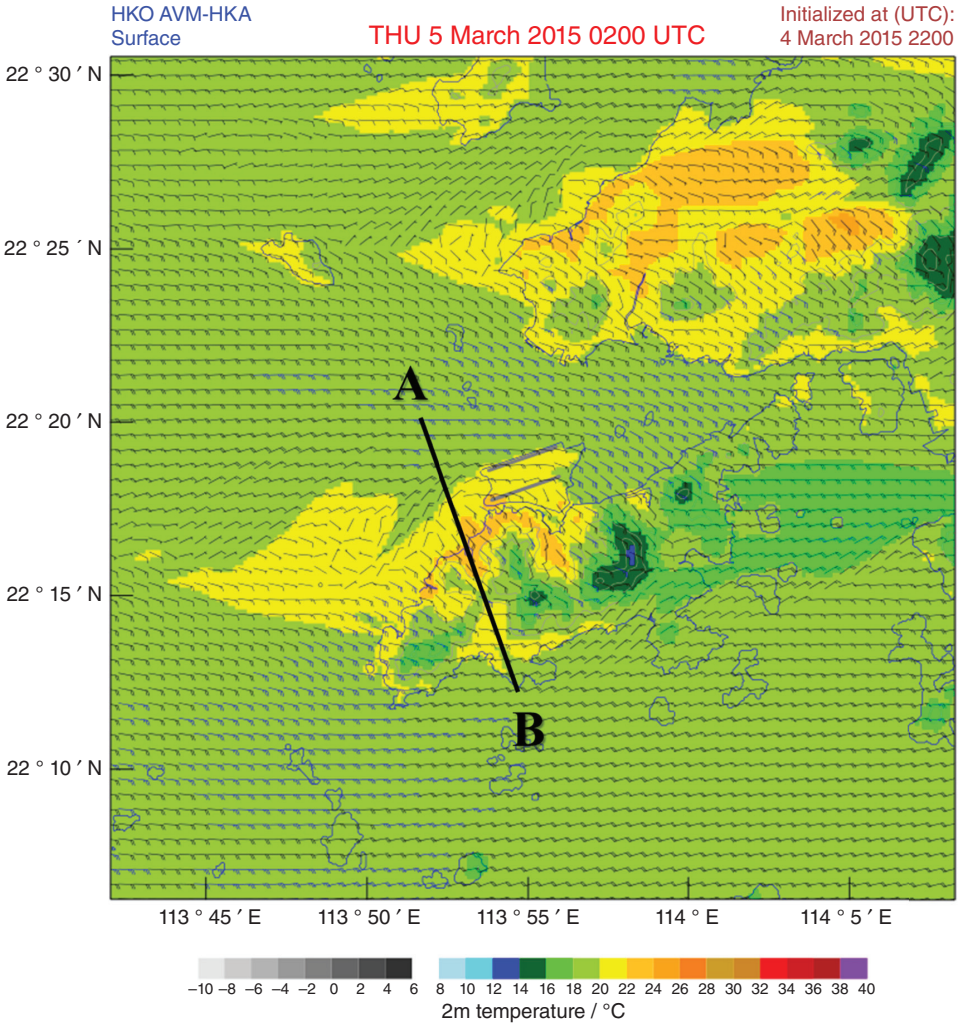

Figure 8. Surface wind and temperature forecast of the aviation model (AVM): 4 h forecast based on 0600 HKT, 5 March 2015. Vertical cross sections in Figure 10 are made from points A to B.

found that, apart from the background east to east-northeasterly flow, there is an area of towards-the-LIDAR system airflow to the southwest of the airport, which is located just downstream of the mountains of Lantau Island. The latter area shows where the radial wind component is towards the LIDAR system. The 0 isodop shows where the radial wind component is 0 m s^{-1} and the wind direction is tangential to the LIDAR system. Thus, the wind direction is southeasterly in the area to the southwest of the airport. This area may be related to the mountain wake and the southerly flow emerging from the valleys of Lantau Island over that region. This mountain wake and the convergence between the southerly and the background easterly flows lead to the occurrence of terrain-induced airflow disturbances over the runway corridors to the west of HKIA (i.e. 07LA). As such, from the headwind profiles collected by the glide-path scans of the LIDAR system, it could be seen that the airflow is rather turbulent and there are many places highlighted with the occurrence of low-level windshear and possible turbulences. In fact, timely windshear alerts have been provided by the LIDAR systems to warn the pilots for all the windshear reports collected in the period 4–5 March 2015.

To examine the performance of the AVM in capturing such terrain-disrupted airflow, first of all, the surface wind and temperature forecasts are examined, and they are shown in Figure 8. Convergence between the background easterly flow and the southerly flow over the western part of Lantau Island is successfully simulated by the model. Moreover, an area of higher temperature is forecast to emanate from the terrain over the western part of Lantau Island to the seas to the west of HKIA. The general features of the Foehn wind are successfully captured by the AVM. Comparing the surface wind patterns of Figure 8 and the actual observations in Figure 5, one major limitation of the model is the under-forecasting of the wind strength at the mountain tops and valleys. The gale force winds as observed in Figure 5 over the western part of Lantau Island are not successfully reproduced in the model simulation.

The GLYGA-AVM results are shown in Figure 9. The simulated LIDAR PPI scan patterns can be found in the middle of each panel. They are similar to the actual observations of the LIDAR system in Figure 7. In particular, the simulation reproduces successfully the salient features of the airflow, namely the background east to southeasterly flow and the convergence between the background flow and the southerly flow over the seas to the west of HKIA. Another observation to be compared is the glide-path scan headwind profiles from the actual LIDAR observations in Figure 7 and the simulated headwinds in Figure 9. Low-level windshear has been successfully forecasted, as highlighted by red coloured ramps in Figure 9. However, the

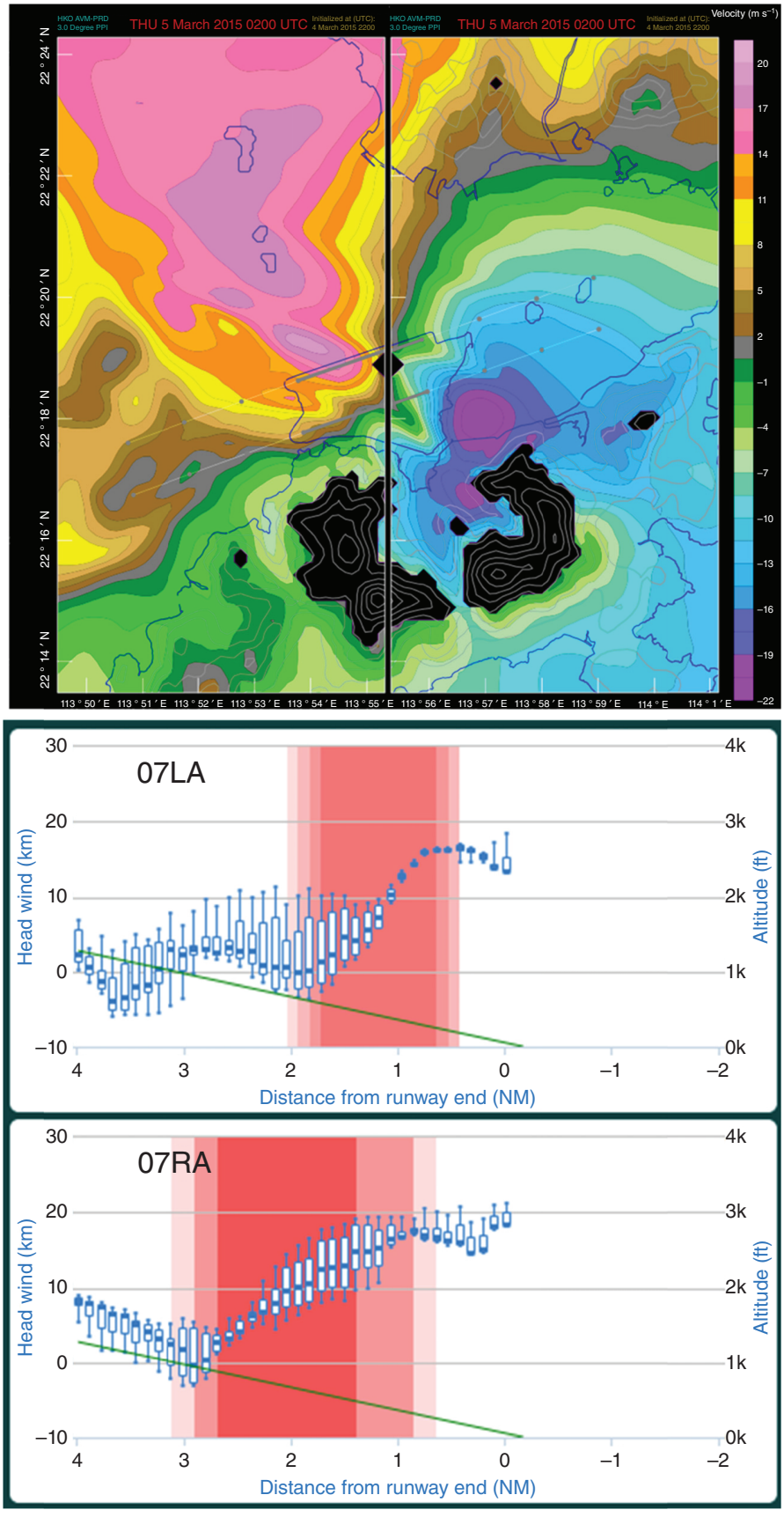

Figure 9. Simulated light detection and ranging (LIDAR) plan position indicator scan (a) and headwind profiles over the western arrival corridors of the Hong Kong International Airport (HKIA) (b) as forecasted by the aviation model (AVM). This case corresponds to the LIDAR observations given in Figure 7. Here, the forecast is valid at 1000 HKT, 5 March 2015, with base time of 0600 HKT, 5 March 2015.

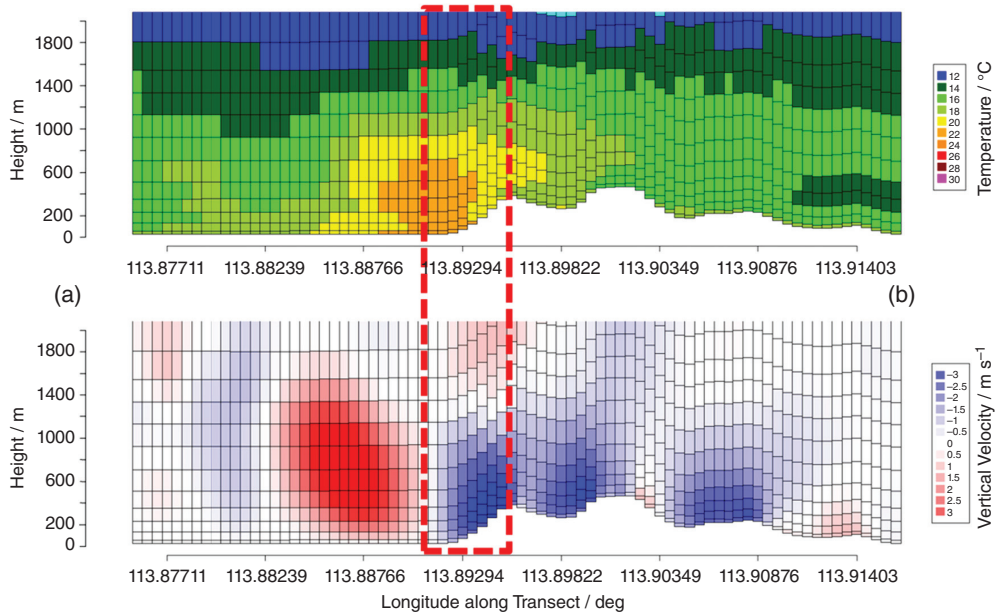

Figure 10. Vertical cross section of temperature (top) and vertical velocity (bottom) between points A and B of Figure 8. Here, model-level data below 2000 m are shown. Data are taken from a 4 h forecast valid at 0600 HKT, 5 March 2015 (same as bottom panel of Figure 9), with a base time of 0600 HKT, 5 March 2015. The region of subsidence warming (orange patch, top panel) associated with the Foehn winds can be seen to follow immediately the strong descending motion downslope of the Lantau hills (highlighted).

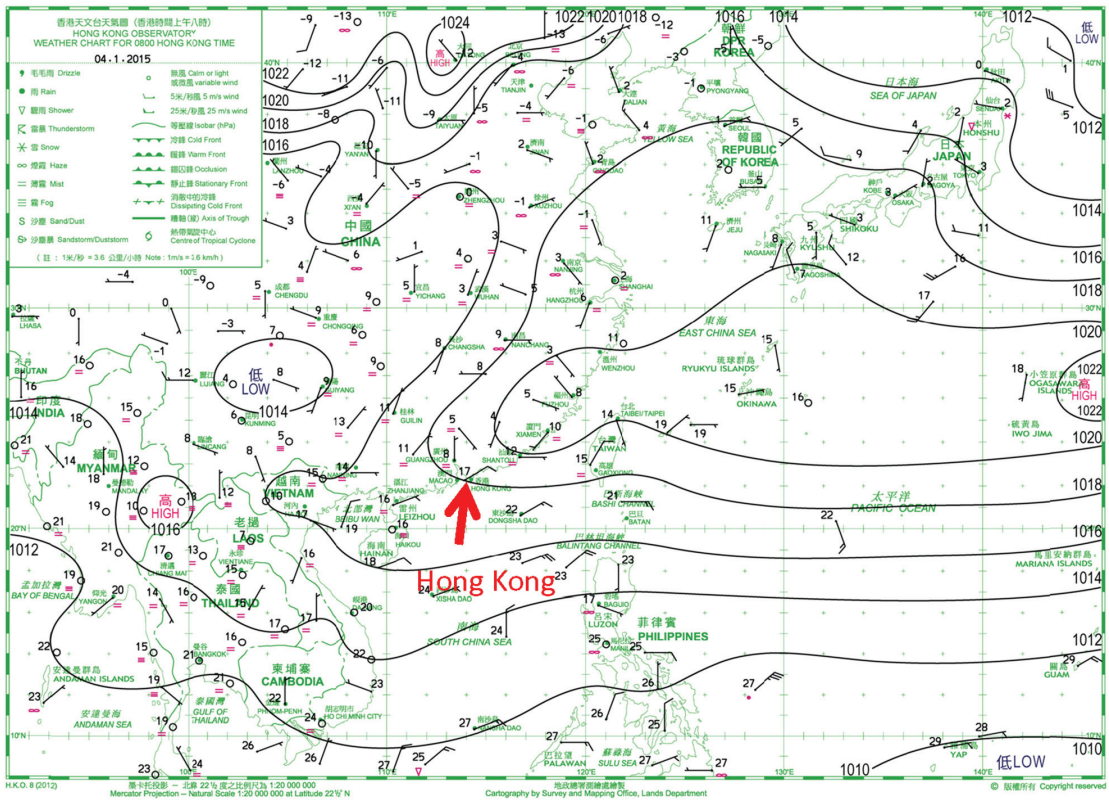

Figure 11. Surface isobaric chart at 0800 HKT on 4 January 2015.

locations and the magnitudes of the ramps are different between the simulations and the observations. This is expected because it would be difficult for the model to simulate the precise location and intensity of the turbulent airflow. Higher resolution NWP model (e.g. at 50 m, as reported in Chan, 2009) and LESs may be required to forecast simulated headwinds that are closer to reality.

To investigate the spatial structure of the Foehn wind effects as simulated by the AVM-HKA, vertical cross sections of winds, temperature and vertical velocity are generated around the western part of Lantau Island, just west of HKIA (Figure 10). The plots run from the northwest to the southeast along the thick black line in Figure 8, such that Point A is to the left and Point B is to

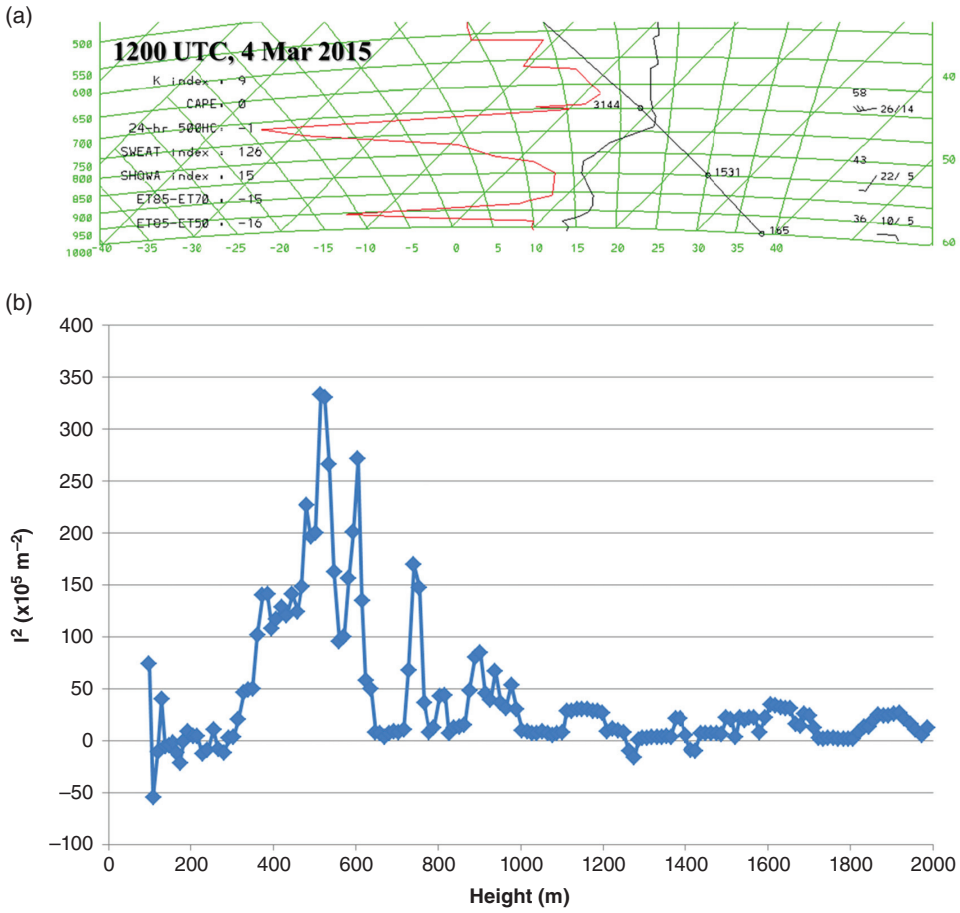

Figure 12. Analysis of King's Park radiosonde data: (a) same as Figure 4 but for the time 2000 HKT, 3 January 2015, and (b) the calculated vertical profile of Scorer's parameter squared.

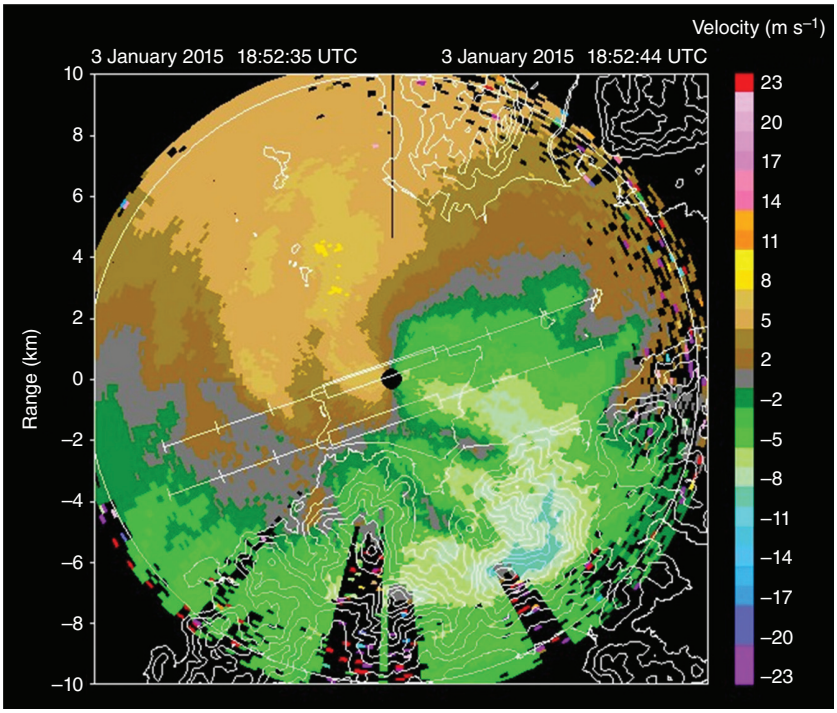

Figure 13. The 6° plan position indicator (PPI) scan of the light detection and ranging (LIDAR) system's radial velocity at 0252 HKT, 4 January 2015.

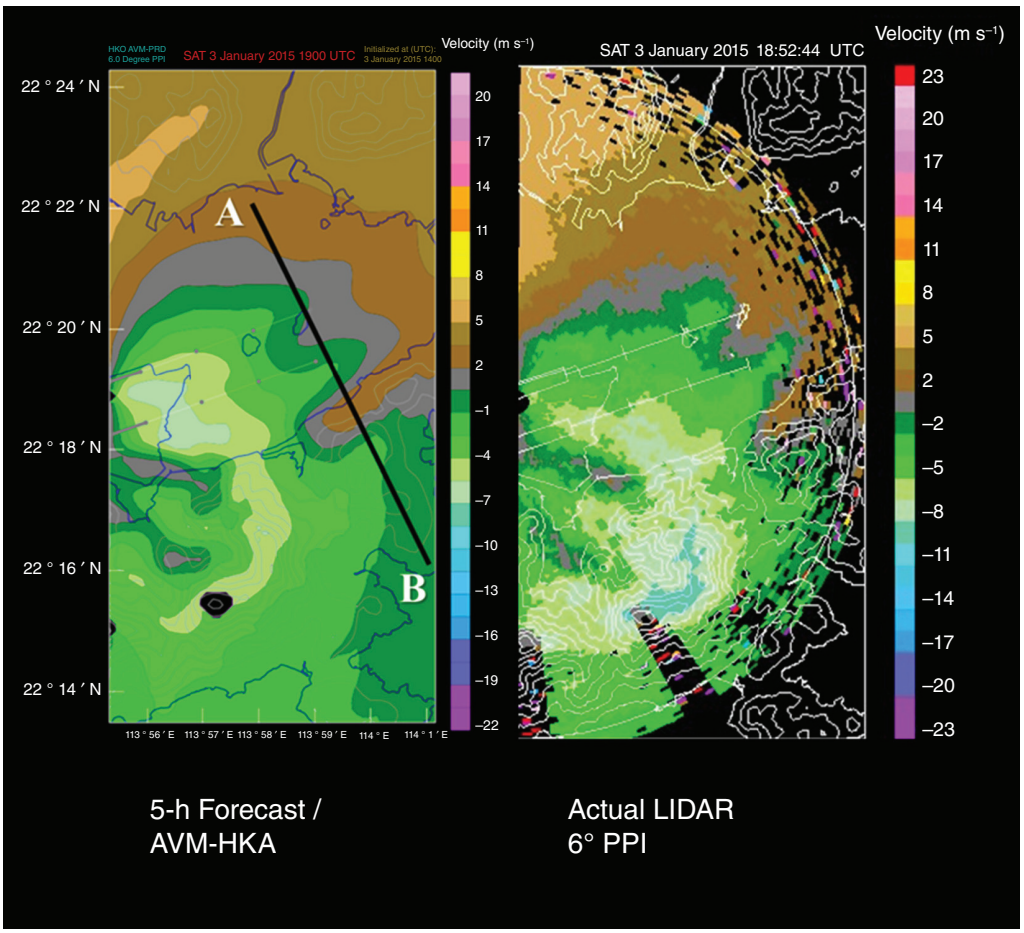

Figure 14. Detailed comparison between simulated (left) and observed (right) 6° light detection and ranging (LIDAR) plan position indicator (PPI) images.

the right. In this sense, the hilly terrain of Lantau Island would mainly lie on the right-hand side of the cross-section plots. The southeasterly winds blowing across Lantau Island would be flowing from the right to the left.

A series of terrain-induced ascent/descent can immediately be seen near the hilly region on the right-hand side of Figure 10. On the upwind (i.e. right) side of each peak, a weak region of forced ascent (in different shades of pink) would occur, with vertical velocities up to 1–2 m s^{-1} (positive for upward motion). This is followed by a downward motion (in different shades of blue) on the leeward side, with vertical velocities between −3 and −2 m s^{-1} (negative for downward motion).

A region of temperature maximum is observed leeward (or to the west) of the leftmost peak (highlighted, near 113.893 ° E), just downstream of an area of strong descending motion. In that region, temperatures can reach 22 to 24 °C (orange), representing an increment of up to 2 to 4 °C from the ambient temperature, which is around 18 to 20 °C (greenish yellow).

4. Mountain wave case

As reported in Shun *et al.* (2004), a stationary mountain wave may occur downstream of Lo Fu Tau, Lantau Island (a hill of about 465 m amsl, Figure 1), when the background east to southeasterly winds are not too strong and there is a temperature inversion at about the height of the hill. Such conditions are fulfilled in the overnight period of 3–4 January 2015. The surface isobaric chart closer to the event time, 0800 HKT, on 4 January is shown in Figure 11. A ridge of high pressure over the southeastern coast of China brought easterly winds to the region. However, compared with the case of the Foehn wind, the pressure gradient of this ridge of high pressure is not so tight. As a result, only moderate easterly winds prevailed at the surface of Hong Kong during the study period.

The background atmospheric condition is shown in the radiosonde ascent at King's Park, Hong Kong, at 2000 HKT, on 3 January (Figure 12(a)). A low-level jet and a temperature inversion are also observed in the radiosonde ascent, but the heights are about the altitude of Lo Fu Tau, ∼400 m amsl. This background condition of the boundary layer would be favourable for the occurrence of a mountain wave downstream of Lo Fu Tau.

The mountain wave is further analysed by considering Scorer's parameter (l) given by (Scorer, 1949):

$$l^2 = (N(z)/U(z))^2 - U_{zz}/U \quad (1)$$

where N is the Brunt-Vaisala frequency, $U(z)$ is the cross-mountain wind speed profile and U_{zz} is the second derivative of U with height z. In the present case, the cross-mountain wind speed increases gradually from 1 to 4 m s^{-1}, and the second term on the right-hand side of Equation (1) may be ignored to a first approximation. The resultant Scorer's parameter squared with height is shown in Figure 12(b). This profile may be approximated by a two-layer model, namely, below a height (h) of ∼1000 m amsl, the mean Scorer's parameter squared (l_1^2) of 6.9×10^{-5} m^{-2} may

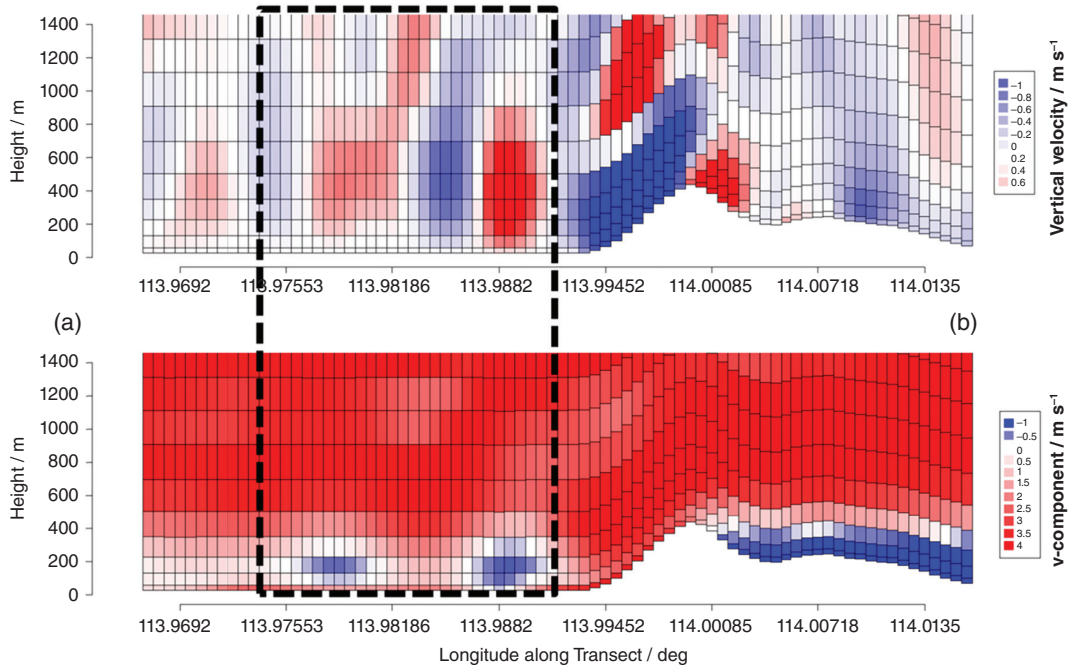

Figure 15. Vertical cross section of vertical velocity (top, red for positive/upwards, blue for negative/downwards) and zonal wind component (bottom, red for positive/southerly, blue for negative/northerly) between points A and B of Figure 14. Here, model-level data below 1400 m are shown. Data are taken from a 5 h forecast valid at 1900 UTC, 3 January 2015 (same as bottom panel of Figure 15), with a base time of 1400 UTC, 3 January 2015. Periodic variations in both vertical velocity and zonal wind component downstream of the Lantau mountains (highlighted) suggested the presence of mountain waves. The asymmetric colour scales are used to highlight the wave-like features.

be adopted. Above this height, the Scorer's parameter squared ($l_2{}^2$) may be taken as 0. As such, it satisfies the following relationship proposed by Scorer (1949):

$$l_1^2 - l_2^2 > \pi/4h^2 \tag{2}$$

The 6° PPI scan from the north runway LIDAR system is shown in Figure 13. East to southeasterly flow prevailed at the airport area from the 3° PPI scan, with the mountain wake (area of green, flow opposite to the background east to southeasterly flow) occurring over the sea to the west of the HKIA. At 6° PPI scan, a mountain wave could be identified downstream of Lo Fu Tau with a zigzag pattern indicated by the LIDAR system's radial velocity.

The GLYGA-AVM display at about the time of the mountain wave occurrence is shown in Figure 14. No windshear is forecast, as consistent with the actual observations. There are headwind changes over the 07RA and 07LA although the change magnitude is less than the threshold of 5 m s^{-1} (10 kn). The PPI scans are given in the middle of the panel. The 3° and 6° PPI patterns are generally consistent with the actual LIDAR observations. In particular, the mountain wake to the west of HKIA and the mountain wave downstream of Lu Fu Tau could be successfully simulated by the AVM-HKA.

In the bottom panel of Figure 14, the 6° LIDAR PPI scan simulated by the AVM-HKA is compared in detail against the northeastern portion of the corresponding LIDAR observation. Firstly, the background flow of easterly to southeasterly winds was in close agreement between the two sources, as indicated by the location and the extent of the green inbound flow south of the LIDAR system's position (i.e. bottom half) and the brown outflow to the north (i.e. near the top of each image). Signature of a wave train can be observed in both images, comprising a number of crests and troughs (alternating green and brown 'fingers') along a northnorthwest–southsoutheast (NNW–SSE) orientation. It can be seen that the intensity (as reflected by the colour scale of simulated and observed Doppler velocity) and the location, as well as the number of wave crests, are reproduced accurately in the AVM-HKA forecast.

To investigate the spatial structure of the simulated mountain waves, vertical cross sections taken along the wave train are shown in Figure 15. Here, the cut is made along the thick black lines in the bottom panel of Figure 14 along a NNW–SSE direction such that point A lies on the left and point B on the right. The two quantities analysed are the vertical velocity w (top, positive for upwards) and the zonal wind component v (bottom, positive for southerly). The asymmetric colour scale is used to highlight the wave-like features.

From the bottom panel of Figure 15, it can be seen that the zonal wind component is generally positive (i.e. from south to north), which is consistent with the known background flow. Downwind (i.e. to the northwest, or left) of Lo Fu Tau, which is the tallest peak shown in the cross section, two regions of flow reversal (blue patches near 113.976° and 113.988° E) can be observed, which correspond to the two green 'fingers' on the simulated Doppler LIDAR velocity images. In the plot of vertical velocity, periodic ascending and descending motion extending to >1000 m is also observed in the downwind area, indicative of the presence of mountain waves. In particular, the locations of maximum updraft coincide with the reversal of zonal wind (highlighted).

5. Conclusion

Two cases of terrain-disrupted airflow occurring at the region around Hong Kong International Airport (HKIA) are investigated in this study. They are typical cases of Foehn wind and mountain wave occurring downstream of Lantau Island. The performance

of the aviation model (AVM) is studied for these two cases. It turns out that the AVM basically captures the main features of the Foehn wind and the associated low-level windshear and turbulence and the mountain wave. Based on the results of this study, it may be possible to use a super high resolution numerical weather prediction model (200 m resolution in the inner domain) to forecast the occurrence of terrain-disrupted airflow under low-level jets and temperature inversions occurring within the atmospheric boundary layer, for the purpose of studying these phenomena and to alert the airport to low-level windshear and turbulence. In particular, the forecasted headwind profiles in the glide-path scan windshear detection algorithm based on the AVM demonstrate skills in forecasting windshear occurrence. The vertical cross sections across the mountains also shed new light on the structures of the terrain-disrupted airflow.

The performance of the AVM over a longer period of time, say 1 year, in the forecasting of upper air winds, windshear and turbulence is presently being studied. The statistical results will be reported in a future publication.

References

Carruthers D, Ellis A, Hunt J, Chan PW. 2014. Modelling of wind shear downwind of mountain ridges at Hong Kong International Airport. *Meteorol. Appl.* **21**: 94–104.

Chan PW. 2009. Atmospheric turbulence in complex terrain: verifying numerical model results with observations by remote-sensing instruments. *Meteorol. Atmos. Phys.* **103**: 145–157.

Chan PW. 2014a. Microwave radiometer measurements of a Foehn wind around Lantau Island, Hong Kong. *Weather* **69**: 93–97.

Chan PW. 2014b. A tail strike event of an aircraft due to terrain-induced wind shear at the Hong Kong International Airport. *Meteorol. Appl.* **21**: 504–511.

Gaffin DM. 2007. Foehn winds that produced large temperature differences near the Southern Appalachian Mountains. *Weather Forecast.* **22**: 145–159.

Hon KK, Chan PW. 2014. Application of LIDAR-derived eddy dissipation rate profiles in low-level wind shear and turbulence alerts at Hong Kong International Airport. *Meteorol. Appl.* **21**: 74–85.

Lee YF, Chan PW. 2014. LIDAR-based F-factor for wind shear alerting: different smoothing algorithms and application to departing flights. *Meteorol. Appl.* **21**: 86–93.

Scorer RS. 1949. Theory of waves in the lee of mountains. *Q. J. R. Meteorol. Soc.* **75**: 41–56.

Shun CM, Chan PW. 2008. Applications of an infrared Doppler Lidar in detection of wind shear. *J. Atmos. Ocean. Technol.* **25**: 637–655.

Shun CM, Lau SY, Cheng CM, Lee OSM, Chiu HY. 2004. LIDAR observations of wind shear induced by mountain lee waves. *11th Conference on Mountain Meteorology and MAP Meeting 2004*, 21–25 June 2004, Mount Washington Valley, NH.

Skamarock WC, Klemp JB. 2007. A time-split nonhydrostatic atmospheric model for weather research and forecasting applications. *J. Comput. Phys.* **227**: 3465–3485.

Wong WK. 2010. Development of operational rapid update non-hydrostatic NWP and data assimilation systems in the Hong Kong Observatory. *The 3th International Workshop on Prevention and Mitigation of Meteorological Disasters in Southeast Asia*, 1–4 March 2010, Beppu, Japan.

Wong WK, Lau CS, Chan PW. 2013. Aviation model: a fine-scale numerical weather prediction system for aviation applications at the Hong Kong International Airport. *Adv. Meteorol.* **2013**: Article ID 532475.